

# Fake It Right: Injecting Anatomical Logic into Synthetic Supervised Pre-training for Medical Segmentation

Jiaqi Tang<sup>1\*</sup>, Mengyan Zheng<sup>2\*</sup>, Shu Zhang<sup>3</sup>, Fandong Zhang<sup>3</sup>, and Qingchao Chen<sup>1\*\*</sup>

<sup>1</sup> Peking University

jiaqi\_tang@hsc.pku.edu.cn, qingchao.chen@pku.edu.cn

<sup>2</sup> Beihang University

zmy050516@buaa.edu.cn

<sup>3</sup> Deepwise Ltd.

{zhangshu, zhangfandong}@deepwise.com

**Abstract.** Vision Transformers (ViTs) excel in 3D medical segmentation but require massive annotated datasets. While Self-Supervised Learning (SSL) mitigates this using unlabeled data, it still faces strict privacy and logistical barriers. Formula-Driven Supervised Learning (FDSL) offers a privacy-preserving alternative by pre-training on synthetic mathematical primitives. However, a critical semantic gap limits its efficacy: generic shapes lack the morphological fidelity, fixed spatial layouts, and inter-organ relationships of real anatomy, preventing models from learning essential global structural priors. To bridge this gap, we propose an **Anatomy-Informed Synthetic Supervised Pre-training** framework unifying FDSL’s infinite scalability with anatomical realism. We replace basic primitives with a lightweight shape bank with de-identified, label-only segmentation masks from 5 subjects. Furthermore, we introduce a structure-aware sequential placement strategy to govern the patch synthesis process. Instead of random placement, we enforce physiological plausibility using spatial anchors for correct localization and a topological graph to manage inter-organ interactions (e.g., preventing impossible overlaps). Extensive experiments on BTCV and MSD datasets demonstrate that our method significantly outperforms state-of-the-art FDSL baselines and SSL methods by 1.74% and up to 1.66%, while exhibiting a robust scaling effect where performance improves with increased synthetic data volume. This provides a data-efficient, privacy-compliant solution for medical segmentation. The code will be made publicly available upon acceptance.

## 1 Introduction

Accurate 3D medical image segmentation is fundamental to clinical diagnosis and treatment planning. While Vision Transformers (ViTs), such as UNETR [4] and

\* These authors contributed equally to this work.

\*\* Corresponding author.

SwinUNETR [3], have demonstrated impressive performance by capturing long-range dependencies, they lack the inductive biases inherent to CNNs [2]. Consequently, these architectures are notoriously data-hungry and prone to overfitting when trained on limited annotations. This creates a critical bottleneck: collecting large-scale, voxel-wise annotated medical datasets is prohibitively expensive, and sharing even unlabeled data is severely restricted by privacy regulations and institutional silos.

To mitigate the dependency on annotated data, *Self-Supervised Learning (SSL)* has emerged as a dominant paradigm. Methods utilizing Masked Image Modeling [13, 5, 18] or contrastive learning [17, 19] leverage vast archives of unlabeled scans to learn robust representations. However, SSL faces two intrinsic limitations. First, it does not circumvent the logistical and legal barriers of data curation, which makes models still require access to large-scale in-domain medical archives. Second, standard SSL objectives, such as intensity reconstruction, primarily focus on local features, often failing to provide explicit supervision. Alternatively, Formula-Driven Supervised Learning (FDSL) [7, 10, 12, 11, 9, 6], offers a privacy-compliant and infinitely scalable solution. By procedurally generating image-label pairs from mathematical rules, FDSL enables the initialization of segmentation models without exposing them to any real patient data. In medical domain, prior works such as PrimGeoSeg [11] constructs 3D volumes by randomly arranging primitive geometric objects (e.g. polygons, cylinders). Nevertheless, a critical *semantic gap* remains between these mathematical primitives and human anatomy. Existing FDSL methods rely on stochastic placement and simplified geometry, failing to capture the **morphological fidelity and fixed topological constraints** inherent in medical scans. For instance, *in a FDSL-generated volume, a cylinder might be randomly positioned above a “lung-like” space, resulting in a spatial configuration that is topologically impossible in human physiology*. Consequently, models pre-trained on such chaotic synthetic data may master low-level edge detection but fail to acquire the essential **anatomical priors**, hindering their ability to distinguish soft tissues with low contrast where spatial context is as important.

To address these limitations, we introduce a hybrid paradigm that merges the infinite scalability of FDSL with the biological validity of real data. We propose an **Anatomy-Informed Synthetic Supervised Pre-training framework**. Unlike SSL approaches that rely on texture reconstruction or generic FDSL methods limited to geometric primitives, our paradigm leverages dense anatomical supervision derived from a generative composition process. To be specific, we introduce a **structure-aware synthesis strategy** by constructing a lightweight shape bank from a minimal set of subjects ( $K = 5$ ) containing only geometric masks, discarding all patient-specific texture information. Instead of random placement, we inject explicit anatomical priors, including class-wise spatial anchors and a topological relation graph to govern the generation. This compels the Transformer to learn valid global anatomical layouts and inter-organ dependencies from scratch, providing strong, pixel-level supervision that is completely privacy-preserving. We systematically evaluate our framework on BTCV [8] and

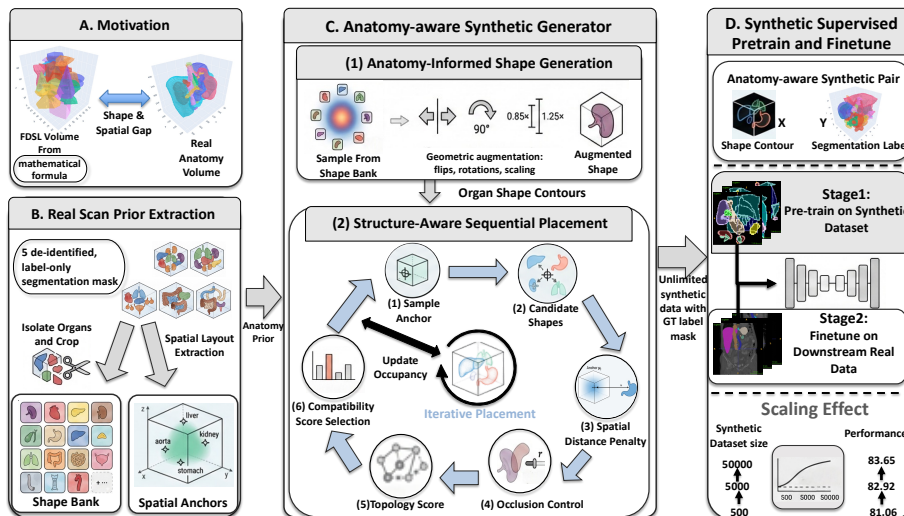


Fig. 1: Overall framework. By extracting morphological and spatial priors from minimal real masks, our generator iteratively synthesizes unlimited, biologically plausible data to bridge the semantic gap of FDSL for robust model pre-training and downstream fine-tuning.

MSD [1] datasets on UNETR [4] and SwinUNETR [3] backbones, outperforming state-of-the-art FDSL baselines and SSL methods by over 1.45% and up to 1.67%.

In summary, we present a novel pre-training paradigm that provides dense, task-aligned supervision without real data. By capturing global structural dependencies unavailable to standard FDSL and demonstrating a continuous scaling effect, our method establishes a robust, privacy-compliant path for data-efficient medical AI.

## 2 Method

Figure 1 illustrates our Anatomy-Informed Synthetic Supervised Pre-training framework, which generates biologically plausible 3D image-label pairs without relying on real patient textures. The pipeline consists of two core components: an anatomy-informed shape bank providing realistic morphological primitives (Sec. 2.2), and a structure-aware sequential placement mechanism governed by spatial and topological constraints (Sec. 2.3). By mathematically formulating this generation as a constrained spatial point process (Sec. 2.1), our method synthesizes diverse, densely annotated volumes to provide robust structural priors for segmentation model pre-training.

## 2.1 Theoretical Formulation

The fundamental objective of synthetic pre-training is to learn a segmentation function  $f_\theta$  minimizing the expected risk on an inaccessible real medical distribution  $\mathcal{D}_{real}$ . Formula-Driven Supervised Learning (FDSL) approximates this via a synthetic distribution  $\mathcal{D}_{syn}$ , generating labeled volume pairs  $(\mathbf{x}, \mathbf{y})$  by sampling  $P(\mathbf{x}, \mathbf{y}) = P(\mathbf{x}|\mathbf{y})P(\mathbf{y})$ . Here, the label  $\mathbf{y}$  comprises shapes  $\mathcal{S}$  and spatial transformations  $\mathcal{T}$ , represented strictly as sets of voxel coordinates. Previous approaches assume shape structures are statistically independent, factorizing the prior as  $P(\mathbf{y}) = \prod P(S_i)P(T_i)$  with uniform  $T_i$ . This unconstrained stochasticity induces a distributional mismatch between  $\mathcal{D}_{syn}$  and  $\mathcal{D}_{real}$ .

To bridge this gap, we propose an **Anatomy-Informed Synthesis** framework redefining  $P(\mathbf{y})$  as a *Constrained Spatial Point Process* governed by a Gibbs distribution conditioned on an anatomical relation graph  $\mathcal{G} = (\mathcal{V}, \mathcal{E})$ :

$$P(\mathbf{y}|\mathcal{G}) = \frac{1}{Z} \exp \left( - \sum_{i \in \mathcal{V}} \psi_{unary}(S_i, T_i) - \sum_{(i,j) \in \mathcal{E}} \psi_{binary}(T_i, T_j) \right)$$

The prior is anchored in valid human physiology while retaining sufficient variance. Two core energy components achieve this:

**Unary Potential**  $\psi_{unary}(S_i, T_i)$ : Encodes a joint shape-position prior. The shape term replaces generic primitives with a non-parametric prior from a lightweight Shape Bank  $\mathcal{B}$  (Sec. 2.2). The positional term replaces uniform placement with an anchor-based penalty  $\psi_{unary}^{pos}(T_i) \propto \|\mathbf{t}_i - \mathbf{a}_i\|_2$ , where the anchor  $\mathbf{a}_i$  is sampled from population statistics  $\mathcal{N}(\mu_i, \Sigma_i)$ . **Binary Potential**  $\psi_{binary}(T_i, T_j)$ : Encodes inter-organ topological dependencies. It penalizes physically impossible overlaps and rewards valid boundary contacts, transforming random placement into a structure-aware composition.

Since exact inference under  $P(\mathbf{y}|\mathcal{G})$  is intractable due to the unnormalized  $Z$ , we approximate the joint distribution via a sequential greedy strategy:  $P(\mathbf{y}|\mathcal{G}) \approx \prod_{t=1}^{|\mathcal{V}|} P(T_t|Y_{t-1}, \mathcal{G})$  where  $Y_{t-1}$  represents the voxel set of previously placed organs. This explicitly bridges our theoretical prior with the tractable candidate ranking generation process detailed in Sec. 2.3. Finally, the image  $\mathbf{x} \sim P(\mathbf{x}|\mathbf{y})$  is rendered as contour shells rather than solid volumes, forcing the encoder to capture structural boundaries invariant to texture, while the supervision labels remain dense, filled volumetric masks.

## 2.2 Anatomy-Informed Shape Generation

Standard FDSL methods rely on simplistic geometric primitives, which fail to capture the complex boundary curvature of human anatomy. To inject realistic morphological priors, we construct a *Shape Bank*  $\mathcal{B}$  derived from a minimal set of real subjects ( $K=5$ ) from TotalSegmentator [16], comprising 32 anatomical classes spanning diverse categories.

To ensure the shapes are clean and reusable, we perform connected component analysis to isolate individual organ instances, followed by bounding-box

cropping with a minimal margin. Crucially, we remap the original discrete class indices to a contiguous range  $\{1, \dots, C\}$ , ensuring a compact label space for the segmentation head. During synthesis, we apply aggressive geometric augmentations, including random flips,  $90^\circ$  rotations, and isotropic scaling within  $[0.85, 1.25]$ —to expand the effective diversity of  $\mathcal{B}$ . This ensures the model learns robust, class-agnostic boundary features rather than memorizing specific patient templates.

### 2.3 Structure-Aware Sequential Placement

To efficiently solve the placement problem without expensive gradient optimization, we employ a Monte Carlo sampling approach with a candidate ranking mechanism. The placement of an organ  $c$  is guided by an *Anatomical Anchor* distribution  $\mathcal{A}_c \sim \mathcal{N}(\boldsymbol{\mu}_c, \boldsymbol{\Sigma}_c)$ , where  $\boldsymbol{\mu}_c$  and  $\boldsymbol{\Sigma}_c$  represent the normalized mean centroid and spatial variance derived from the training corpus.

For each instance, we first sample a specific anchor point  $\mathbf{a} \sim \mathcal{A}_c$ . We then generate a set of  $N$  candidate poses  $\Pi = \{\pi_j\}_{j=1}^N$  by sampling random perturbations around  $\mathbf{a}$ . The optimal pose  $\pi^*$  is selected by maximizing a discrete scoring function  $S(\pi)$  that aggregates spatial, physical, and topological fidelity:

$$\pi^* = \arg \max_{\pi_j \in \Pi} [S_{spatial}(\pi_j, \mathbf{a}) + S_{phys}(\pi_j, Y_{t-1}) + S_{topo}(\pi_j, Y_{t-1}, \mathcal{G})]. \quad (1)$$

The **Spatial Fidelity** term  $S_{spatial}$  enforces the generated organ to remain close to the sampled anatomical anchor. It is defined as the negative Euclidean distance  $S_{spatial} = -\lambda_{anc} \|\mathbf{t}_\pi - \mathbf{a}\|_2$ , where  $\mathbf{t}_\pi$  is the centroid of the candidate mask. This acts as a stochastic tether, ensuring global anatomical correctness while allowing for natural variation.

The **Physical Constraint** term  $S_{phys}$  penalizes unnatural overlaps with the currently occupied volume  $Y_{t-1}$ . We define this as  $S_{phys} = -\lambda_{ovl} \cdot \text{IoU}(\mathbf{m}^\pi, Y_{t-1})$ , where IoU denotes the Intersection-over-Union ratio. Furthermore, we enforce a hard constraint for biologically incompatible pairs (e.g., bone vs. viscera) defined in the exclusion set  $\mathcal{E}_{avoid}$ . If  $\text{IoU}(\mathbf{m}^\pi, Y_{prev}^{(k)}) > \tau_{hard}$  for any  $k \in \mathcal{E}_{avoid}$ , the candidate is immediately rejected by setting  $S(\pi) = -\infty$ .

To model inter-organ interactions, we introduce a **Topological Score** term  $S_{topo}$  governed by a relation graph  $\mathcal{G}$ . This term encourages specific geometric relationships via indicator functions. For containment relationships (e.g., trachea inside lung), we reward candidates where the inclusion ratio exceeds a threshold  $\tau_{in}$ . Similarly, for adjacency relationships (e.g., liver contacting aorta), we reward candidates that exhibit sufficient boundary contact voxels:

$$S_{topo} = \sum_{(c,k) \in \mathcal{E}_{in}} \lambda_{in} \mathbb{I} \left( \frac{|\mathbf{m}^\pi \cap Y^{(k)}|}{|\mathbf{m}^\pi|} > \tau_{in} \right) + \sum_{(c,k) \in \mathcal{E}_{adj}} \lambda_{adj} \mathbb{I} \left( |\partial \mathbf{m}^\pi \cap Y^{(k)}| > \nu_{contact} \right). \quad (2)$$

By maximizing this composite score, the generator selects the candidate that best balances random variation with anatomical plausibility. The final volume

Table 1: Comparison of segmentation performance on the BTCV dataset. The best results are highlighted in bold.

Pre-training	PT Num	Avg.	Spl	RKid	LKid	Gall	Eso	Liv	Sto	Aor	IVC	Veins	Pan	rad	lad
<i>UNETR</i>															
Scratch	0	75.86	93.02	89.79	90.60	51.34	71.12	95.02	72.90	82.95	76.71	69.05	76.29	62.02	55.33
PrimGeoSeg [11]	5K	78.90	93.19	93.47	93.35	54.49	68.91	95.88	78.83	87.82	82.47	72.73	80.08	65.06	59.35
Ours	5K	<b>80.64</b>	<b>94.23</b>	<b>93.61</b>	93.32	<b>62.66</b>	<b>71.76</b>	95.79	<b>80.51</b>	<b>90.13</b>	<b>84.11</b>	<b>73.67</b>	79.98	<b>66.49</b>	<b>62.08</b>
<i>SwinUNETR</i>															
Scratch	0	80.12	95.32	94.01	93.51	61.17	73.83	94.40	71.19	88.13	85.20	73.12	80.60	67.15	63.88
PrimGeoSeg [11]	5K	80.08	95.25	93.76	93.79	61.23	74.47	96.04	80.64	89.39	83.91	74.27	77.83	64.13	56.36
Ours	5K	<b>81.53</b>	94.39	<b>94.26</b>	<b>93.87</b>	59.18	<b>74.92</b>	<b>96.67</b>	80.00	<b>90.46</b>	<b>85.22</b>	<b>74.59</b>	<b>82.88</b>	<b>68.06</b>	<b>65.45</b>

is constructed by sequentially overlaying the selected masks in descending order of their volumes, simulating the occlusion effects inherent in medical imaging.

### 3 Experiments

#### 3.1 Experimental Setup

**Tasks and datasets:** We evaluate on both CT and MRI modalities to assess cross-modal generalization. *For CT*, we use BTCV [8] (multi-organ) and MSD [1] Task06 (Lung) and Task09 (Spleen). *For MRI*, we evaluate on MSD Task02 (Heart). This MRI evaluation is particularly important as it tests whether anatomical priors learned from synthetic CT pre-training transfer to a different imaging modality without explicit MRI pre-training data. All datasets are split 80/20 for training/validation, and experiments are conducted offline.

**Data Synthesis Setting:** We construct shape bank  $\mathcal{B}$  from  $K=5$  TotalSegmentator [16] subjects with geometric augmentation (flip  $p=0.5$ ,  $90^\circ$  rotation, scaling  $[0.85, 1.25]$ ). Structure-aware placement uses  $N_c=40$  candidates per organ with thresholds  $r=0.7$ ,  $\sigma=0.12$ ,  $\tau=0.35$ , contact minimum  $v_{\min}=20$ , and containment ratio 0.30. Compatibility weights are  $w_o = -1.0$ ,  $w_a=0.8$ ,  $w_c=w_t=1.0$ .

**Training details:** During pre-training, we use a ROI size of  $96 \times 96 \times 96$ , a batch size of 4, a learning rate of 0.0002, and a weight decay of 0.00001. The model is optimized using AdamW with a warmup cosine learning rate scheduler. The pre-training dataset contains 5K samples, and the number of training iterations is set to 25000. For fine-tuning on the BTCV and MSD datasets, we follow the standard hyperparameter settings used in prior works [11] with a batch size of 4. All downstream experiments are evaluated using the Dice similarity coefficient.

#### 3.2 Results and Analysis

**BTCV Multi-Organ Segmentation.** As shown in Tables 1, for BTCV [8] dataset, on UNETR, our method achieves 80.64% average Dice, surpassing the scratch baseline by 4.78% and PrimGeoSeg by 1.74%. Substantial improvements in structures with weak boundaries (e.g., gallbladder +11.32%, stomach +7.61%) demonstrate that our anatomical priors effectively compensate for ambiguous

Table 2: Comparison of segmentation performance on the MSD dataset across different pre-training strategies. Results are reported for both UNETR and SwinUNETR architectures.

Method	MSD Dataset					
	Task 02		Task 06		Task 09	
	UNETR	SwinUNETR	UNETR	SwinUNETR	UNETR	SwinUNETR
Scratch	95.14	95.34	70.68	76.14	92.52	95.92
PrimGeoSeg	95.61	95.77	78.81	80.39	<b>96.30</b>	96.96
<b>Ours</b>	<b>96.02</b>	<b>95.93</b>	<b>80.47</b>	<b>81.45</b>	96.20	<b>97.38</b>

Table 3: Comparison with Self-Supervised Learning (SSL) methods pre-trained on real medical datasets. All models use the SwinUNETR backbone and are fine-tuned on BTCV. (Note: values differ slightly from Table 1 due to foreground cropping during fine-tuning, but relative improvements remain consistent.)

Method	Pre-train Data	Data Amount	Avg. Dice
Scratch	None	0	80.12
SwinMM [15]	Real (CT)	5,000	76.72
SwinUNETR [14]	Real (CT)	5,000	80.56
PrimGeoSeg	Synthetic	5,000	80.08
<b>Ours</b>	<b>Synthetic</b>	<b>5,000</b>	<b>81.51</b>

appearance cues. For SwinUNETR, our method achieves the best overall performance (81.53%), yielding superior accuracy in complex vascular and glandular organs. Notably, PrimGeoSeg fails to surpass the scratch baseline here (80.08% vs. 80.12%), indicating that generic primitives lack the structural complexity needed to initialize sophisticated hierarchical transformers.

**MSD Benchmark Generalization.** Our method also exhibits robust cross-dataset and cross-modal transferability, validated on the MSD [1] dataset. On Task06 (Lung), our method consistently outperforms both the scratch baseline and the state-of-the-art FDSL method (PrimGeoSeg). Specifically, for UNETR, we achieve a substantial improvement of 9.79% over training from scratch and 1.66% over PrimGeoSeg. Similarly, SwinUNETR sees gains of 5.31% and 1.06% respectively. Crucially, our method demonstrates effective generalization to MRI (Task02 Heart) despite the synthetic pre-training data being derived exclusively from CT. By achieving 96.02% (UNETR) and 95.93% (SwinUNETR), our approach sets a new state-of-the-art, validating that the spatial relationships and topological constraints learned through our structure-aware synthesis are inherently modality-invariant.

**Scaling Effect.** We evaluate the impact of synthetic data volume (500, 5,000, and 50,000) on UNETR’s downstream BTCV performance (Fig. 2). Our framework consistently outperforms the scratch baseline (80.02%), achieving 81.06%,

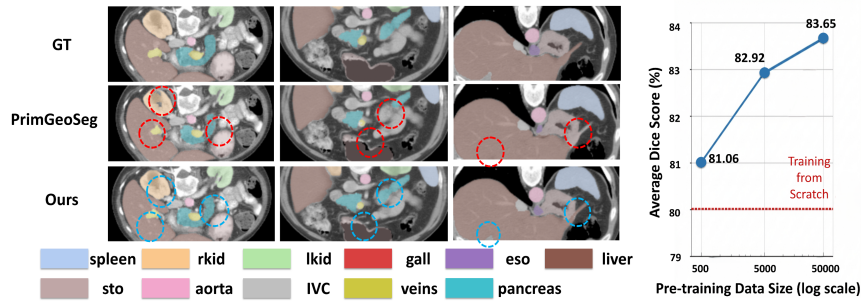


Fig. 2: **Left:** Qualitative comparison results. Red dashes indicate misidentified areas and blue dashes indicate more accurately identified areas. **Right:** Scaling effect when controlling the generated data number from 500 to 50000.

82.92%, and 83.65% average Dice, respectively. The marginal gain diminishes as data scales (+1.86% from 500 to 5,000 vs. +0.73% from 5,000 to 50,000), indicating that 5,000 samples offer a practical trade-off between computational cost and accuracy.

**Comparison with SSL Methods.** We compare our approach against state-of-the-art self-supervised learning methods pre-trained on real medical data (Table 3). Using SwinUNETR on BTCV, our anatomy-informed synthetic pre-training (81.51%) surpasses both the scratch baseline and PrimGeoSeg. Remarkably, it also exceeds SwinUNETR [14] pre-trained on 5,000 real CT volumes (80.56%). In contrast, reconstruction-based SSL like SwinMM [15] underperforms the scratch baseline (76.72%), suggesting that masked reconstruction objectives may struggle to capture precise semantic features under subtle domain shifts. These results demonstrate that dense, pixel-level anatomical supervision from structured synthetic data is highly effective, offering a privacy-compliant alternative that outperforms unsupervised representation learning on sensitive real scans.

## 4 Conclusion

In this paper, we presented an Anatomy-Informed Synthetic Supervised Pre-training framework that bridges the infinite scalability of Formula-Driven Supervised Learning (FDSL) with the biological realism of medical scans. By enforcing physiological plausibility and topological constraints through a structure-aware composition strategy, our method significantly outperforms state-of-the-art self-supervised and generic synthetic baselines across multiple CT and MRI benchmarks. Crucially, our work validates a highly promising technical route: *dense, pixel-level synthetic supervision injected with explicit anatomical logic can effectively substitute the reliance on massive, privacy-sensitive real-world datasets.* This paradigm demonstrates that structural priors are more critical than texture

reconstruction for medical pre-training, establishing a scalable, data-efficient, and strictly privacy-compliant foundation for training robust 3D medical Transformers in data-limited scenarios.

## References

1. Antonelli, M., Reinke, A., Bakas, S., Farahani, K., Kopp-Schneider, A., Landman, B.A., Litjens, G., Menze, B., Ronneberger, O., Summers, R.M., et al.: The medical segmentation decathlon. *Nature communications* **13**(1), 4128 (2022)
2. Dosovitskiy, A.: An image is worth 16x16 words: Transformers for image recognition at scale. *arXiv preprint arXiv:2010.11929* (2020)
3. Hatamizadeh, A., Nath, V., Tang, Y., Yang, D., Roth, H., Xu, D.: Swin unetr: Swin transformers for semantic segmentation of brain tumors in mri images (2022), <https://arxiv.org/abs/2201.01266>
4. Hatamizadeh, A., Tang, Y., Nath, V., Yang, D., Myronenko, A., Landman, B., Roth, H.R., Xu, D.: Unetr: Transformers for 3d medical image segmentation. In: *Proceedings of the IEEE/CVF Winter Conference on Applications of Computer Vision*. pp. 574–584 (2022)
5. He, K., Chen, X., Xie, S., Li, Y., Dollár, P., Girshick, R.: Masked autoencoders are scalable vision learners (2021), <https://arxiv.org/abs/2111.06377>
6. Kataoka, H., Hayamizu, R., Yamada, R., Nakashima, K., Takashima, S., Zhang, X., Martinez-Noriega, E.J., Inoue, N., Yokota, R.: Replacing labeled real-image datasets with auto-generated contours. In: *Proceedings of the IEEE/CVF conference on computer vision and pattern recognition*. pp. 21232–21241 (2022)
7. Kataoka, H., Matsumoto, A., Yamada, R., Satoh, Y., Yamagata, E., Inoue, N.: Formula-driven supervised learning with recursive tiling patterns. In: *Proceedings of the IEEE/CVF International Conference on Computer Vision*. pp. 4098–4105 (2021)
8. Landman, B., Xu, Z., Igelsias, J., Styner, M., Langerak, T., Klein, A.: Miccai multi-atlas labeling beyond the cranial vault—workshop and challenge. In: *Proc. MICCAI multi-atlas labeling beyond cranial vault—workshop challenge*. vol. 5, p. 12. Munich, Germany (2015)
9. Nakamura, R., Kataoka, H., Takashima, S., Noriega, E.J.M., Yokota, R., Inoue, N.: Pre-training vision transformers with very limited synthesized images. In: *Proceedings of the IEEE/CVF International Conference on Computer Vision*. pp. 20360–20369 (2023)
10. Shinoda, R., Hayamizu, R., Nakashima, K., Inoue, N., Yokota, R., Kataoka, H.: Segrcdb: Semantic segmentation via formula-driven supervised learning. In: *Proceedings of the IEEE/CVF international conference on computer vision*. pp. 20054–20063 (2023)
11. Tadokoro, R., Yamada, R., Kataoka, H.: Pre-training auto-generated volumetric shapes for 3d medical image segmentation. In: *Proceedings of the IEEE/CVF Conference on Computer Vision and Pattern Recognition*. pp. 4740–4745 (2023)
12. Takashima, S., Hayamizu, R., Inoue, N., Kataoka, H., Yokota, R.: Visual atoms: Pre-training vision transformers with sinusoidal waves. In: *Proceedings of the IEEE/CVF Conference on Computer Vision and Pattern Recognition*. pp. 18579–18588 (2023)

13. Tang, Y., Yang, D., Li, W., Roth, H.R., Landman, B., Xu, D., Nath, V., Hatamizadeh, A.: Self-supervised pre-training of swin transformers for 3d medical image analysis. In: Proceedings of the IEEE/CVF Conference on Computer Vision and Pattern Recognition (CVPR). pp. 20730–20740 (June 2022)
14. Tang, Y., Yang, D., Li, W., Roth, H.R., Landman, B., Xu, D., Nath, V., Hatamizadeh, A.: Self-supervised pre-training of swin transformers for 3d medical image analysis. In: Proceedings of the IEEE/CVF Conference on Computer Vision and Pattern Recognition. pp. 20730–20740 (2022)
15. Wang, Y., Li, Z., Mei, J., Wei, Z., Liu, L., Wang, C., Sang, S., Yuille, A.L., Xie, C., Zhou, Y.: Swinmm: masked multi-view with swin transformers for 3d medical image segmentation. In: International conference on medical image computing and computer-assisted intervention. pp. 486–496. Springer (2023)
16. Wasserthal, J., Breit, H.C., Meyer, M.T., Pradella, M., Hinck, D., Sauter, A.W., Heye, T., Boll, D.T., Cyriac, J., Yang, S., Bach, M., Segeroth, M.: Totalsegmentator: Robust segmentation of 104 anatomic structures in ct images. *Radiology: Artificial Intelligence* **5**(5) (Sep 2023). <https://doi.org/10.1148/ryai.230024>, <http://dx.doi.org/10.1148/ryai.230024>
17. Wu, L., Zhuang, J., Chen, H.: Voco: A simple-yet-effective volume contrastive learning framework for 3d medical image analysis (2024), <https://arxiv.org/abs/2402.17300>
18. Xie, Z., Zhang, Z., Cao, Y., Lin, Y., Bao, J., Yao, Z., Dai, Q., Hu, H.: Simmim: A simple framework for masked image modeling (2022), <https://arxiv.org/abs/2111.09886>
19. Zhou, Z., Sodha, V., Siddiquee, M.M.R., Feng, R., Tajbakhsh, N., Gotway, M.B., Liang, J.: Models genesis: Generic autodidactic models for 3d medical image analysis (2019), <https://arxiv.org/abs/1908.06912>